J. Water Environ. Nanotechnol., 6(4): 294-305 Autumn 2021

ORIGINAL RESEARCH PAPER

Synthesis and Characterization of Novel $Mg(OH)_2$/CdS Hetero Nanostructures for Sunlight-Induced Degradation of Phenolic Pollutant

Aishwarya Singh, Bhavani Prasad Nenavathu*

[1] Department of Applied Sciences and Humanities, Indira Gandhi Delhi Technical University for Women, Delhi, 110006, India

Received: 2021-06-15 Accepted: 2021-08-01 Published: 2021-09-01

ABSTRACT

Mg(OH)2/CdS hetero nanostructures have been successfully synthesized by a novel precipitation method and the synthesis involves three steps. The first step involves the synthesis of $Mg(OH)_2$ nanoparticles using the homogeneous precipitation method. Then, surface-modifying agent citric acid was used to functionalize Mg $(OH)_2$. Finally, the cadmium sulfide (CdS) shell was deposited on the surface-modified Mg $(OH)_2$ by the co-precipitation method. The $Mg(OH)_2$/CdS hetero nanostructures were characterized using X-ray diffraction, scanning electron microscopy (SEM), transmission electron microscopy (TEM), diffuse reflectance spectroscopy (DRS), and photoluminescence spectroscopy. DRS results indicated a blue shift of CdS bandgap absorption with respect to the bulk CdS. XPS results showed evidence for the binding energies of $Mg(OH)_2$, Cd, and S. The Mg $(OH)_2$/CdS hetero nanostructures were explored as a catalyst for sunlight-induced photocatalytic degradation of β- naphthol pollutant. The 0.2 mg/ mL batch of Mg $(OH)_2$/CdS hetero nanostructures maintained at pH 8.5 showed maximum photodegradation efficiency (75 ± 2.1 %). Higher photocatalytic degradation efficiency for $Mg(OH)_2$/CdS hetero nanostructures could be due to the incorporation of CdS and increased reactive oxygen species (ROS) generation. The reusability of the Mg $(OH)_2$/CdS hetero nanostructures was also tested, indicating stability for up to three cycles without any loss of efficiency.

Keywords: *chemical precipitation method, $Mg(OH)_2$/CdS hetero nanostructures, nanoneedles, cauliflower-shaped, β- naphthol pollutant, Photocatalysis*

How to cite this article

Singh A., Nenavathu B.P. Synthesis and Characterization of Novel $Mg(OH)_2$/CdS Hetero Nanostructures for Sunlight-Induced Degradation of Phenolic Pollutant . J. Water Environ. Nanotechnol., 2021; 6(4): 294-305.

DOI: 10.22090/jwent.2021.04.001

INTRODUCTION

Water contamination is one of the major problems of the whole world and it is due to industrial and radioactive wastes, inadequate sewage treatment, marine dumping issues, etc. [1,2]. $Mg(OH)_2$ nanomaterials being nontoxic, noncorrosive, eco-friendly, and highly stable have been used earlier for water purification [3, 4]. There have been various methods reported for the synthesis of $Mg(OH)_2$ nanoparticles and their nanocomposites. $Mg(OH)_2$ nanopowders having platelet-like morphology were synthesized from the serpentinite mineral via solvothermal reaction [5]. However, Mg $(OH)_2$ use is restricted to the UV region due to its wide bandgap. Some studies were carried out to narrow down the band gap of semiconductors by coupling them with metals, to use them in the visible region. In this respect, cobalt was doped into Mg $(OH)_2$ nanoparticles (NPs) using the co-precipitation method for narrowing the bandgap of Mg $(OH)_2$[6]. In this scenario, $Mg(OH)_2$/2 dimensional (2D) heterostructures such as $Mg(OH)_2/MoS_2$, $Mg(OH)_2/WS_2$, $Mg(OH)_2$/AlN were found to be useful due to their optical and electronic properties [7-9]. Blue P/$Mg(OH)_2$ heterostructures were used as an efficient visible

* Corresponding Author Email: *bhavaniprasadnaik@igdtuw.ac.in*

photocatalyst for water splitting [10]. $CuInS_2$/ $Mg(OH)_2$ nanosheets were synthesized via hydrothermal approach and used for enhanced visible-light photocatalytic degradation of Tetracycline antibiotic [11]. Zero valent iron supported on $Mg(OH)_2$ was synthesized by the chemical precipitation method for the enhanced removal of Pb(II) from an aqueous solution [12]. Carbon cloth-supported $Mg(OH)_2$ were synthesized via electrodeposition and were used for rare earth metal Europium (□) recovery from an aqueous solution [13]. High-gravity technology was used for the fabrication of $Mg(OH)_2$/graphene oxide composite and was used for the removal of dyes [14]. TiO_2 / $Mg(OH)_2$ hetero nanostructures were synthesized by simple thermal hydrolysis method and used for the catalytic degradation of chemical warfare agents DMMP, 2-CEES, and 2-CEPS [15]. A strong light absorptive $Mg(OH)_2$ micro flowers supported by Ruthenium nanoparticles were synthesized for the photothermal carbon dioxide hydrogenation [16]. In order to convert the UV-based photocatalyst like Mg $(OH)_2$ to visible photocatalyst and to obtain extraordinary optical and electronic properties, it is necessary to couple it with the semiconductors having a narrow bandgap. Furthermore, the separation of photoexcited electron-hole pairs could be achieved using $Mg(OH)_2$ based heterostructure. In this regard, CdS is a tremendous preference since it has a bandgap of about 2.42 eV, and also combining it with large bandgap materials, could induce excellent optical and electrical properties [17]. The characteristics such as morphology, electronic and optical properties of the nanomaterials need to be considered for attaining good efficiency in applications like photocatalysis, water splitting, etc. under natural sunlight [18-20]. Besides, Mg $(OH)_2$/ CdS heterostructures were capable of transferring their charge from one semiconductor to another leading to the prevention of exciton recombination, simultaneously tuning the bandgap of Mg $(OH)_2$ to the visible region. Commonly, during the synthesis of nanoparticles, citric acid, a tridentate carboxylic acid, was used as a stabilizing ligand. The excellent characteristics possessed by the citrate ions are good surface binding capacity, prevention of agglomeration, and bringing water solubility to the synthesized nanoparticles. β-naphthol, one of the naphthalene derivatives, which is widely used in industrial chemicals and used extensively in dyestuffs manufacturing, pharmaceutical production, and biogeochemical processes is found to be hazardous. This compound's maximum allowable limit from the effluent of the factories is 3 ppm [21]. The techniques based on the usage of biological methods, membranes, and evaporation methods, which have been carried out to eliminate β-naphthol in water have some limitations due to secondary environmental pollution [22]. In this regard, Praseodymium oxide nanostructures were prepared via a thermal treatment approach and their photocatalytic activity was investigated by the degradation of 2-naphthol under ultraviolet light irradiation [23]. Nanocrystalline cadmium molybdate was prepared by ultrasonic method their photocatalytic degradation against 2-naphthol under visible light irradiation was carried out [24]. Both the rutile and anatase forms of TiO_2 nanoparticles stabilized on activated carbon using microwave energy were synthesized and used in the removal of β-naphthol from wastewater, under A 20 W power UV-C light [21]. N-TiO_2/SiO_2 and nitrogen-doped N-TiO_2/SiO_2 were prepared by sol-gel method and their photocatalytic activities against β-naphthol were evaluated with a 25 W lamp (Natural light PT 2191-ExoTerra) as the simulated solar light source [25].

In this paper, we present a simple, economical method for the synthesis of Mg $(OH)_2$/CdS hetero nanostructures and were characterized and further explored as sunlight-driven photocatalysts for the degradation of β-naphthol in an aqueous solution.

- Synthesis of $Mg(OH)_2$/CdS hetero nanostructures using a simple, economical, chemical precipitation method
- Characterization of synthesized material using X-ray diffraction, scanning electron microscopy (SEM), transmission electron microscopy (TEM), diffuse reflectance spectroscopy (DRS), and photoluminescence spectroscopy, etc.
- Sunlight-induced photocatalytic degradation of β- naphthol pollutant.
- Determination of hydroxyl radicals using the terephthalic acid assay.
- Determination of the role of Histidine as reactive oxygen species (ROS) scavenger.

EXPERIMENTS

Materials

β-naphthol, Sodium sulfide were purchased from SRL Chem Ltd., India. Magnesium Nitrate (Fischer), citric acid (99 %, Himedia, LR), cadmium chloride (99 %, Lobachemiepvt. Ltd., AR), sodium

hydroxide (98 %, Rankem, AR), Mercaptoacetic acid (MAA) (Fischer), Terephthalic acid (CDH chemicals), acetone (99 %, Qualigens) was used as received.

Synthesis of $Mg(OH)_2$/CdS hetero nanostructures

The $Mg(OH)_2$/CdS hetero nanostructures were synthesized using the following three steps

Synthesis of $Mg(OH)_2$ nanoparticles

A standard solution of 0.1M concentration of magnesium nitrate was prepared by dissolving 6.41gm of magnesium nitrate in 25mL of water and was stirred at 80 ^{0}C for 1 h to obtain a clear solution. Then the uniform solution of 0.1 M NaOH was added drop by drop to the above solution. Further, the resultant mixture was stirred for an extra 2h, to attain completion of the reaction. Then, the resultant solution was collected and centrifuged for 15 min at 5000 rpm and washed with sterilized double-distilled water. Finally, the obtained white precipitate was dried in a hot air oven at 70 ^{0}C overnight.

Surface modification of $Mg(OH)_2$ NPs

The surface modification of $Mg(OH)_2$ nanoparticles was carried out using citric acid as the surface-modifying agent. Initially, $Mg(OH)_2$ of concentration 1 mM was prepared by dissolving 0.8 gm of $Mg(OH)_2$ in 50 mL of distilled water and then 0.05gm of citric acid was added. The obtained mixture was stirred at room temperature for 4 h. The contents formed were filtered, washed, and dried in the oven at 70 ^{o}C.

Synthesis of $Mg(OH)_2$/CdS heteronanostructures using precipitation method

To 50 mM $CdCl_2$ aqueous solution, 87.2 µL of mercaptoacetic acid (MAA) was added dropwise. The above solution was stirred for 30 min. The pH of the resulting solution was raised to 8.0 using 0.1 N NaOH. Further, $Mg(OH)_2$ was added to the above solution and then the aqueous suspension of sodium sulfide was added and stirred for 3 h. Further, acetone was added, to precipitate the synthesized hetero nanostructures. Finally, the nanocomposite was separated by centrifuging at 4000 rpm for 5 min. The supernatant was discarded and the yellow-colored precipitate so obtained was washed with deionized water and centrifuged. The obtained residue was stored at room temperature till further use. This batch of the sample will be henceforth referred to as $Mg(OH)_2$/CdS hetero nanostructures.

Characterization of $Mg(OH)_2$/CdSheteronanostructures

The X-ray diffraction measurements of the $Mg(OH)_2$/CdS hetero nanostructures were performed with (M. Smartlab, Rigaku) operated at 40 kV using graphite monochromatized Cu K_α radiation source with a wavelength of 1.54 Å in a wide-angle region from 10° to 90° on a 2θ scale. The morphology of $Mg(OH)_2$/CdS hetero nanostructures were characterized by using field emission scanning electron microscopy coupled with energy dispersive X-ray analyzer VY.05 (SIGMA). The absorption spectroscopy of the as-synthesized nanoparticle dispersion was measured by UV–vis spectrophotometer (Cary 100 UV Vis) in the range of 200–800 nm shown in Table 1. The bandgap of the synthesized hetero nanostructures was determined from diffuse reflectance spectra (Shimadzu, UV-2450) with $BaSO_4$ as the reference scattering material. The emission spectra are recorded using a fluorescence spectrophotometer (Shimadzu, RF-5301 PC) at an excitation wavelength (λex) of 315 nm. The excitation and emission slit width of 5 nm was maintained for all the measurements. The chemical constituents in the $Mg(OH)_2$/CdS hetero nanostructures were determined from X-ray photoelectron spectroscopy (XPS) using a multi-technique surface analysis system of Omicron Nanotechnology, Germany. The XPS analyses were carried out using a monochromatic Al Kα X-ray source of 1486.7 eV, with an operating voltage of 15 kV and emission current of 15 mA. The samples for XPS analysis of $Mg(OH)_2$/CdS hetero nanostructures were made as pellets using a hydraulic press. The transmission electron microscopy (TEM) images were recorded using FEI Technai-G^2 microscope

Table 1. Crystallite size, absorption maxima and Bandgap of Pristine $Mg(OH)_2$ NPs and $Mg(OH)_2$/CdS NC

Photocatalyst	$\lambda_{max(nm)}$	Crystallite size (nm)	Band gap (eV)
Pristine $Mg(OH)_2$ NPs	238	14	5.50
$Mg(OH)_2$/CdS NC	404	3	2.45

operated at 200 kV and its corresponding nature was determined by SAED attachment. The samples for TEM analysis were prepared by placing a drop of diluted $Mg(OH)_2$/CdS hetero nanostructures dispersed on a carbon-coated 150 mesh copper grid and dried at room temperature.

Photocatalytic degradation study

The degradation of β-naphthol– a model pollutant was studied using $Mg(OH)_2$/CdS hetero nanostructures under natural sunlight. In our study, β-naphthol pollutant of 7 x 10^{-5} M was prepared, and the batches of the test solution were treated with Mg $(OH)_2$/CdS hetero nanostructures (MC) of increasing concentrations of 0.1mg/mL (MC1), 0.2 mg/mL(MC2), 0.3 mg/mL of Mg $(OH)_2$/CdS hetero nanostructures (MC3) and compared with bare Mg $(OH)_2$ NPs and control sample (without nanoparticles). The pollutant treated with different batches of NPs was first ultrasonicated for 20 min in dark to ensure minimal ROS formation and followed by stirring for 40 min for proper adsorption and desorption equilibrium. All the batches of test solutions were continuously stirred in the presence of sunlight between 12:00 noon and 2:00 pm at IGDTUW campus, Delhi in March 2021 when the intensity of the sunlight fluctuation is low. The intensity of sunlight at Delhi (the latitude 28° 40' 2.96" N and longitude 77° 13' 40.96" E respectively) in March is 1366 Watt/m^2.

The time-dependent degradation studies of the pollutant were carried out by measuring the concentration of a pollutant from the test sample at an interval of 30 min. The obtained aliquot was centrifuged at 15000 rpm at 25 °C for 5 min in Beckman Coulter™Allegra™ X-22 R to separate the dispersed nanoparticles and its absorption maxima were measured at λabs=223 nm. The decomposition of the pollutant was compared with a positive control containing the same concentration of pollutants without NPs. The effect of degradation of pollutant by Mg $(OH)_2$/CdS was also compared with a negative control containing the same concentration of pollutant treated with Mg $(OH)_2$ NPs. An experiment was performed in the absence of sunlight, to study the effect of light. All analyses were performed in triplicate and the results are presented as mean and standard deviation of three analyses.

Measurement of OH radicals (ROS indicator)

The batches of 0.2 mg/mL each of Mg $(OH)_2$ NPs and Mg $(OH)_2$/CdS hetero nanostructures were sonicated for 10 min in 3 mM solution of terephthalic acid prepared in 0.01 M NaOH solution. The obtained solution was continuously stirred for 30 min to form adducts between terephthalic acid and OH* radicals. The dispersed solution was centrifuged at 7000 rpm for 5 min and the emission spectrum of the supernatant was recorded using Shimadzu fluorescence spectrophotometer (RF-5301 PC) at an excitation wavelength (λ_{exc}) of 315 nm. A control experiment was carried out by measuring the intensity of the emission spectrum of the reaction mixture before UV illumination. The total number of OH radicals generated during the reaction was a measure of the fluorescence intensity of adducts formed between the OH radical and terephthalic acid [26]. All analyses were performed in triplicate and the results are presented as mean and standard deviation of three analyses.

RESULTS AND DISCUSSION

XRD patterns of pure Mg $(OH)_2$ and Mg $(OH)_2$/CdS hetero nanostructures were shown in Fig. 1. Pure Mg $(OH)_2$nanostructures (JCPDS file No: 00-044-1482) [7] showed reflections at 18.77°, 32.90°, 38.04°, 50.90°, 58.68°, 62.09°, 68.31°, 72.17°and 81.33° are ascribed to (001), (100), (101), (102), (110), (111), (103), (201) and (202) planes respectively. The intense peak at 2θ = 38.04°confirmed the preferred orientation of Mg $(OH)_2$ facet along the (101) plane. Pure CdS showed reflections at 26.44°, 43.80°, and 52.00° corresponding to (111), (220), and (311) planes of cubic CdS (JCPDS file no: 01-080-0019) [27] (Fig. S1.) In the XRD patterns of Mg $(OH)_2$/CdS hetero nanostructures, both Mg $(OH)_2$ and CdS reflections are observed. Fig. 1b. shows that the XRD peaks due to CdS in the hetero nanostructures are more intense and less broad. The crystallite size of Mg $(OH_)_2$ and CdS in the Mg $(OH)_2$/CdS samples was calculated using Debye–Scherrer equation using the XRD peaks at 2θ = 38.04° for Mg $(OH)_2$ (101) and at 2θ = 26.44° for CdS (111). The average crystallite size of pure Mg $(OH)_2$ is higher (14 nm) compared to that in the Mg $(OH)_2$/CdS hetero nanostructures (3 nm approx.).

The FE-SEM images of Mg $(OH)_2$/CdS samples are shown in Fig. 2. Pure Mg $(OH)_2$ showed platelet-like morphology, after surface modification with citric acid (Fig.S2). In the presence of citric acid, the crystallinity and precipitation dispersibility of

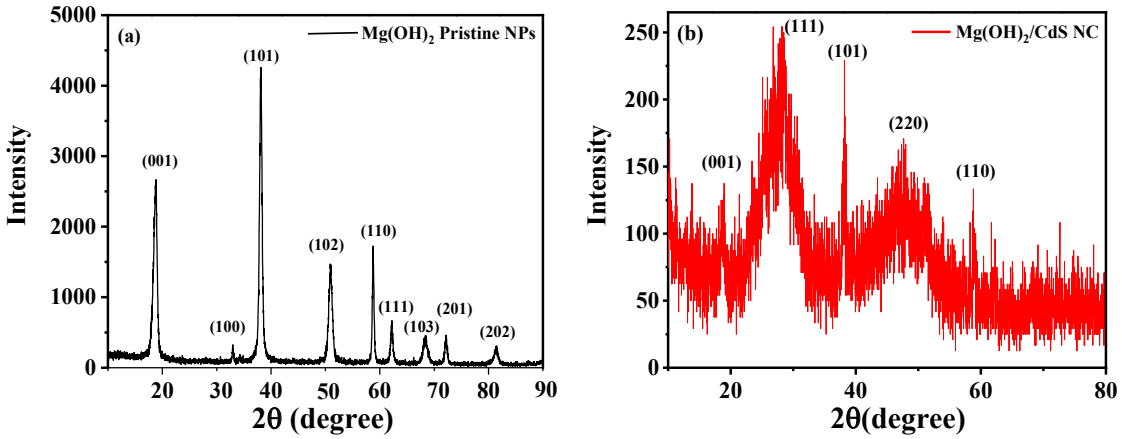

Fig. 1. XRD patterns of (a) pristine $Mg(OH)_2$ NPs (b) $Mg(OH)_2$/CdS heteronanostructures

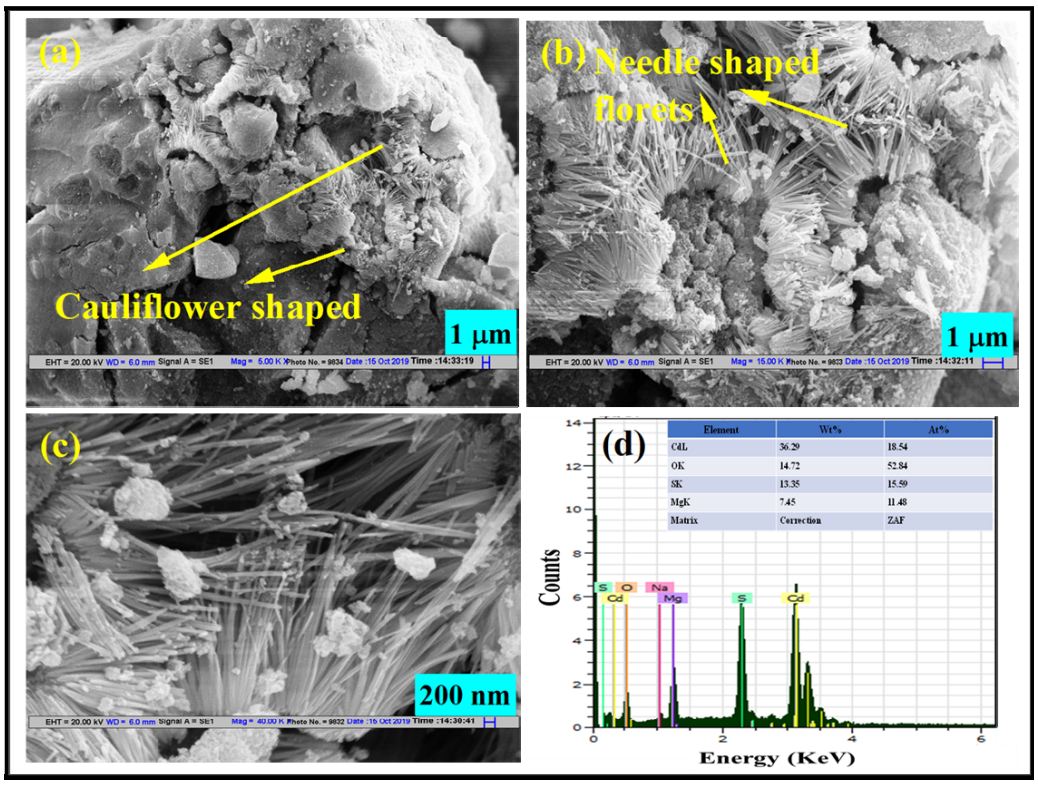

Fig. 2. (a)-(c) Showing Scanning electron microscopy of $Mg(OH)_2$/CdS hetero nanostructures and (d) showing energy dispersive X-ray analysis of $Mg(OH)_2$/CdS hetero nanostructures

Mg $(OH)_2$ was improved drastically [28]. In the final step of the synthesis, using the precipitation method, nanoneedles were obtained. Our results were in good agreement with the following data [29]. Herein the crystal growth was observed, in which the length of Mg $(OH)_2$nanoneedles was about 1000 nm and the diameter was found to be 20 ± 5 nm. It was also observed that some of the agglomerated CdS nanoparticles got deposited irregularly on the surface of Mg $(OH)_2$. The elemental composition of Mg $(OH)_2$/CdS hetero nanostructures was studied using EDX analysis (Fig. 2d). All the samples showed the presence of elements such as Mg, O, Cd, S, etc. The TEM and

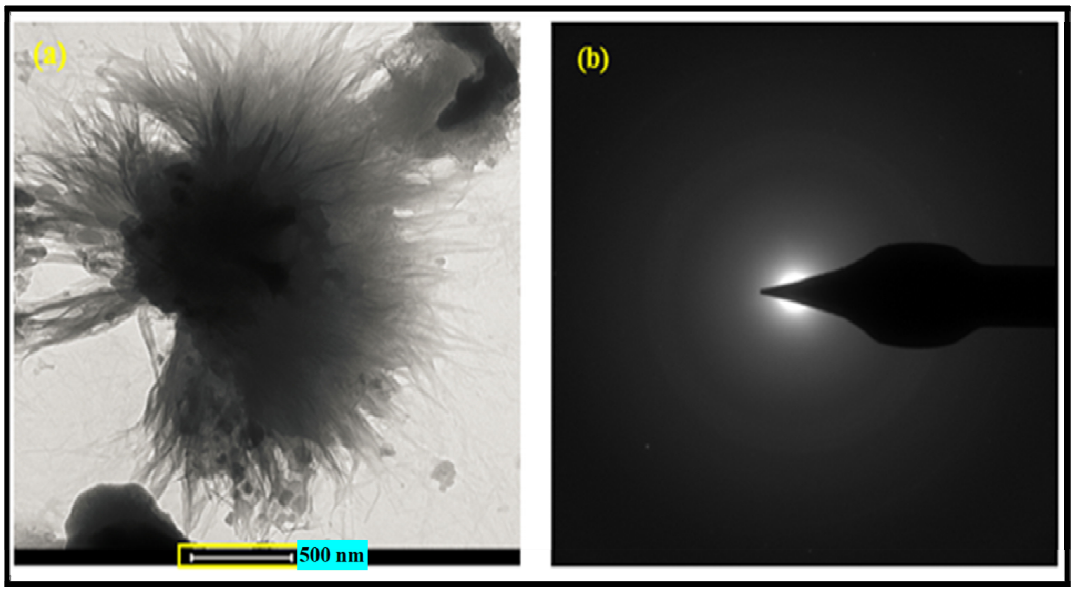

Fig. 3. (a) Showing Transmission electron microscopy of $Mg(OH)_2$/CdS hetero nanostructures (b) SAED of $Mg(OH)_2$/CdS hetero nanostructures

SAED images of $Mg(OH)_2$/CdS samples were shown in Fig.3. The SAED patterns of Mg $(OH)_2$/CdS hetero nanostructures confirmed the amorphous nature of the material and this could be due to the higher deposition of CdS NPs on the surface of Mg $(OH)_2$ /CdS. Moreover, from the XRD pattern of CdS, as shown in Fig. S1. it's clear that the obtained CdS nanomaterial was amorphous. Further, the determination of chemical state and chemical composition of Mg $(OH)_2$/CdS sample was studied by XPS (Fig. 4), where Mg, O, Cd, S binding energy peaks and their oxidation states were revealed. Fig. 4a shows the detailed scan of Mg $(OH)_2$ /CdS heteronanostructures, wherein the characteristic peaks of Mg (KLL), Cd 3p,3d, O 1s, and S2p were observed. Mg showed a binding energy peak at 51 eV corresponding to 2p(Fig.4c), which confirmed the presence of Mg^{+2}. Further, the binding energy value of 1304eV was observed for Mg 1s(Fig.4d) and the value 50.5 eV was related to Mg-O/OH species in the spectra. For O 1s the Binding energy value 532.6 eV was observed(Fig.4b), which proved the existence of hydroxide form [30]. Similarly, the binding energy peaks of Cd $3d_{3d5/2}$ and Cd $3d_{3d3/2}$ were recorded at 407eV and 412 eV and for S2p it was recorded at 161.5 eV and 162.7 eV, which showed the presence of sulfur in S^{2-} form (Fig.4e,f). Our results corroborated well with the following data [31].

The DRS and absorption spectra of Mg $(OH)_2$ /CdS hetero nanostructures were shown in Fig. 5. The bandgap values of pure Mg $(OH)_2$ /CdS hetero nanostructures were calculated using the Kubelka-Munk plot. Pure Mg $(OH)_2$ and CdS have direct bulk band gap values of 5.7 and2.42 eV respectively [7,32]. In the present study, pure Mg $(OH)_2$ / CdS hetero nanostructures possess a bandgap of 2.45 eV. The Mg $(OH)_2$ in the Mg $(OH)_2$/CdS hetero nanostructures showed about 3.1 eV blue shift with respect to bulk Mg $(OH)_2$ (Eg = 5.5 eV). In Mg $(OH)_2$/CdS hetero nanostructures, the blue shift of the bandgap absorption of CdS is ascribed to the quantum size effect [33]. The absorption maxima showed two peaks in $Mg(OH)_2$/CdS samples which were found to be 238 nm and 408 respectively (Fig.5a). The higher catalytic activity could be achieved through efficient charge separation.

Photocatalytic activity: effect of sunlight and concentration of the photocatalyst

The degradation kinetics of β-naphthol by the batches of Mg $(OH)_2$/CdS hetero nanostructures were studied for 2.5 h and were compared with the photodegradation of the control batch, where inβ-naphthol was not treated with nanoparticles (data shown in Fig. 6a). The pollutant was treated with photocatalyst Mg $(OH)_2$/CdS hetero nanostructures (MC)of increasing concentrations of 0.1 mg/mL (MC1), 0.2 mg/mL (MC2), 0.3 mg/mL of Mg $(OH)_2$/CdS hetero nanostructures (MC3)

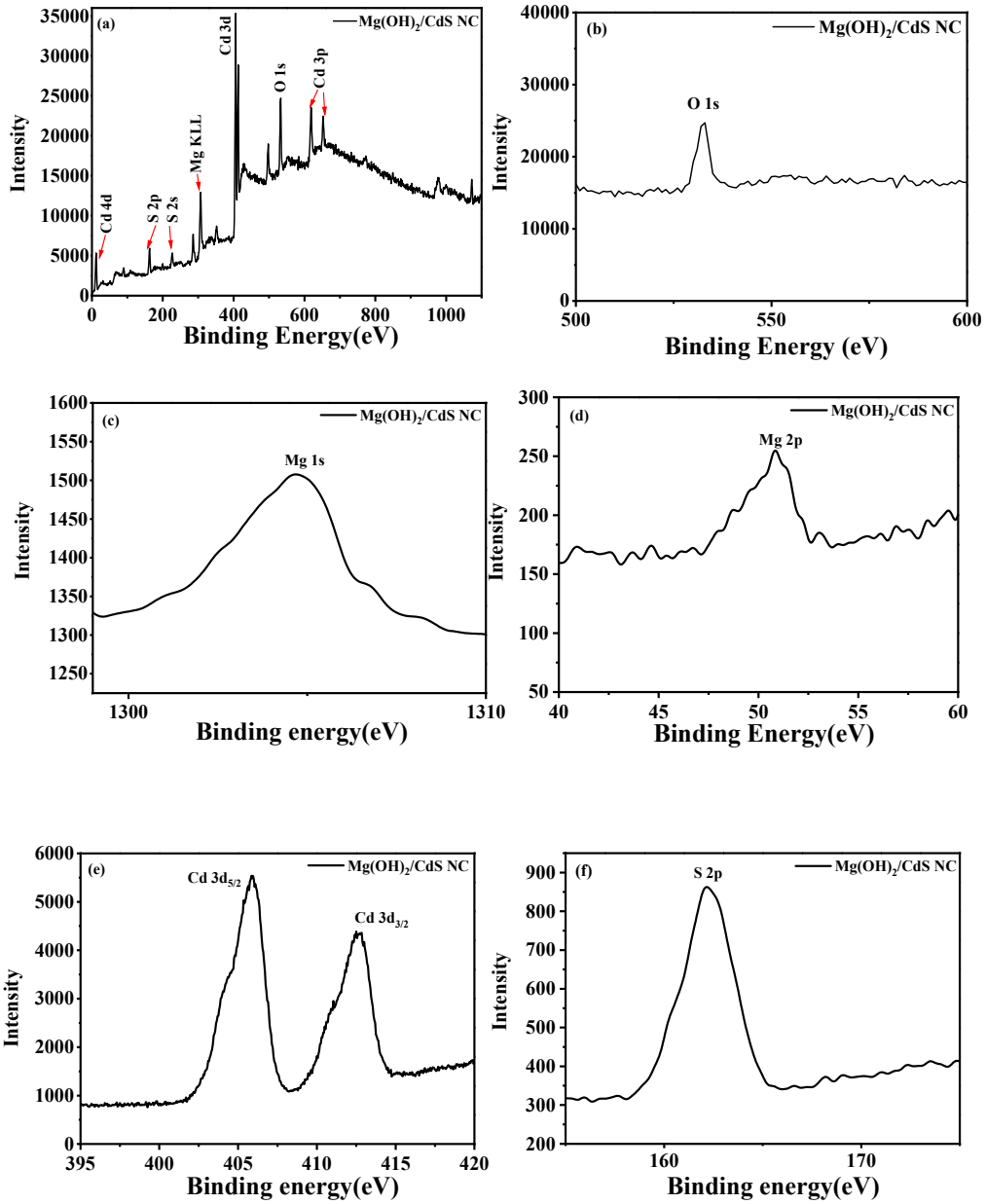

Fig. 4. XPS of Mg(OH)$_2$/CdS hetero nanostructures showing chemical composition and oxidation state of the synthesized material (a) Combined Binding energy peaks of Mg KLL, S 2s and 2p, Cd 3d and 3p, O 1s (b) Binding energy of O 1s (c)and (d) Binding energy of Mg 1s and 2p respectively (e) Binding energy of Cd 3d (f) Binding energy of S 2p

and compared with bare Mg (OH)$_2$ NPs and control sample (without nanoparticles). The kinetics of β-naphthol degradation was also studied (Fig. 6b). The higher photocatalytic activity was shown by Mg (OH)$_2$/CdS hetero nanostructures compared to pure Mg (OH)$_2$ platelets (Fig.6b). Photodegradation of β-naphthol followed first-order kinetics and is evident from the linear relationship between ln (Co/C) and irradiation time in Mg (OH)$_2$/CdS hetero nanostructures [34,35]. The noticeable first-order rate constant (k) for the degradation of β-naphthol was calculated as 0.005, 0.009, 0.009 min^{-1} for MC1, MC2, MC3 respectively showing no further increase in efficiency for MC3. Among all three samples, the highest degradation efficiency and rate constant were shown by MC2 and MC3 samples making MC2 the optimum concentration.

The photodegradation efficiencies of Mg (OH)$_2$/

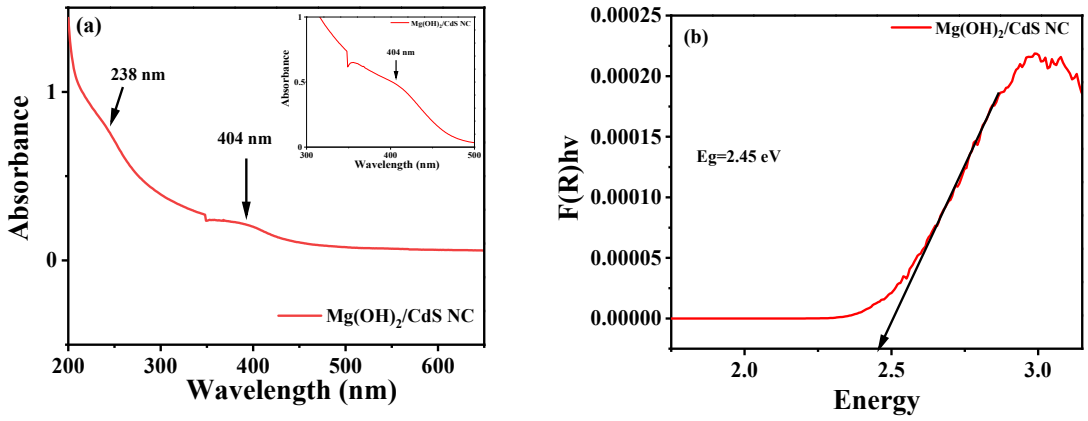

Fig. 5. (a) Showing Absorption maxima and (b) Bandgap using K-M plot of Mg(OH)$_2$/CdS hetero nanostructures

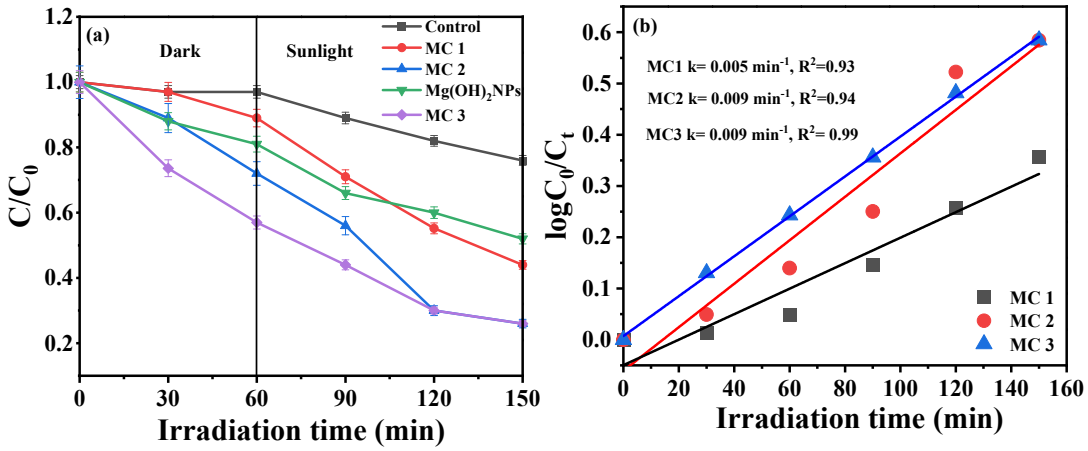

Fig. 6. (a) comparison of photocatalytic performance of both Pristine and Mg(OH)$_2$/CdS hetero nanostructures (b) plots of ln(Co/C) versus irradiation time for various photocatalysts

CdS hetero nanostructures of 0.2 mg/mL were determined to be 75 ± 3.4 %, which followed first-order kinetics (Fig. 6b) and were much higher than that of the Mg (OH)$_2$ of the same concentration (52 ± 1.2 %). It may be remarked here that the batch of 0.3 mg/mL of Mg (OH)$_2$/CdS hetero nanostructures did not show a considerable increase in the degradation efficiency (75 ± 2.8 %). Absorption spectra of degradation of β-naphthol in natural light was shown in Fig. S3. However, after particular catalyst content, a reduction in the penetration of the light has been observed in the solution due to the creation of opacity; Consequently, a decrease in the number of radicals leading to a slight decrease in the degradation efficiency was noticed. In the absence of sunlight, the degradation of β-naphthol by Mg (OH)$_2$/CdS (MC2), through adsorption was found to be 27.8 ± 1.5% after 1h.

Mechanism of β-naphthol degradation

When sunlight illuminated on Mg (OH)$_2$/CdS hetero nanostructures, electrons (e^-) and holes (h^+) were generated. The produced excitons either recombine or create superoxide radicals ($O_2^{\bullet -}$) due to electron-mediated reduction of surface oxygen. Subsequently, hydroxyl radicals (OH*) were generated, which might act as primary oxidants for catalyzing the degradation reaction of dyes and organic compounds [36,37]. Therefore e^- h^+ recombination needs to be suppressed to attain efficient photocatalytic degradation. When Mg (OH)$_2$/CdS samples are exposed to sunlight, the transfer of electrons from the conduction band of CdS to that of Mg (OH)$_2$ has occurred facilitating the prevention of electron-hole pair recombination. The conduction band of Mg (OH)$_2$ possesses more electrons and no free holes were

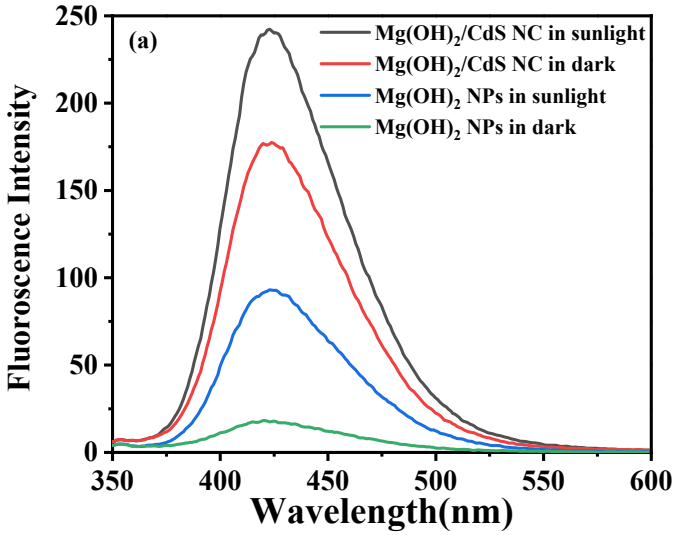

Fig. 7. Determination of hydroxyl radicals during the photocatalytic degradation of **β-naphthol** under sunlight using photoluminescence spectroscopy

available in the valence band of $Mg(OH)_2$ for the recombination. The electrons could be utilized for the reduction of oxygen bound to the surface of $Mg(OH)_2$ and resulted in the formation of highly reactive superoxide anions followed by generation of reactive oxygen species (ROS), e.g., hydroxyl radical (OH•). Similarly, the holes can oxidize adsorbed water on the CdS to form highly reactive hydroxyl radical (OH•), and eventually participate in photocatalytic degradation of β-naphthol.

The possible mechanism for the photodegradation of β-naphthol was given in Scheme 1. In the present case, the real VB and CB of $Mg(OH)_2$/CdS hetero nanostructures and bare $Mg(OH)_2$ and CdS have been estimated theoretically

$$E_{VB} = X - 4.5 + 0.5\, E_g$$

$$E_{CB} = E_{VB} - E_g$$

Here, E_{VB}, E_{CB}, and E_g correspond to the valence band, conduction band, and bandgap of the individual semiconductor. X represents the geometrical summation of individual elements of the corresponding semiconductor. The VB and CB of $Mg(OH)_2$/CdS hetero nanostructures and bare $Mg(OH)_2$ and CdS are presented in Table S1. The observed VB and CB band positions indicate that $Mg(OH)_2$/CdS possess a lower conduction band and lower valence band than bare $Mg(OH)_2$, which facilitates fast electron transport to the surface and enhances the photocatalytic activity towards photodegradation of β-naphthol.

ROS induced photocatalytic effect by $Mg(OH)_2$/CdS hetero nanostructures

Nanoparticles usually generate reactive oxygen species (ROS) in water, when they interact with light [38]. In the present study, hydroxyl radicals were generated upon the interaction of 0.2 mg/mL $Mg(OH)_2$/CdS hetero nanostructures dispersed in aqueous media. The formation of OH* was detected by the terephthalic acid assay and was corroborated well with the data corresponding to hydroxyl radical-mediated dye degradation using Se doped ZnO NPs [39]. The intensity of the fluorescent emission peak measured at λnm= 425 nm corresponds to the formation of an adduct between terephthalic acid and the OH* generated in the aqueous media. The order of the emission peak intensities was found to be $Mg(OH)_2$/CdS>$Mg(OH)_2$ as shown in Fig.7, which also follows the same tendency for the order of OH* formed in the reaction mixture. Further, the amount of OH* generated was found to be more, when the reaction was carried out in the presence of sunlight compared to dark conditions. This indicated that the higher photodegradation efficiency of $Mg(OH)_2$/CdS was due to higher OH* generation in aqueous media.

In order to ascertain the role of ROS generation toward photodegradation of β-naphthol, an

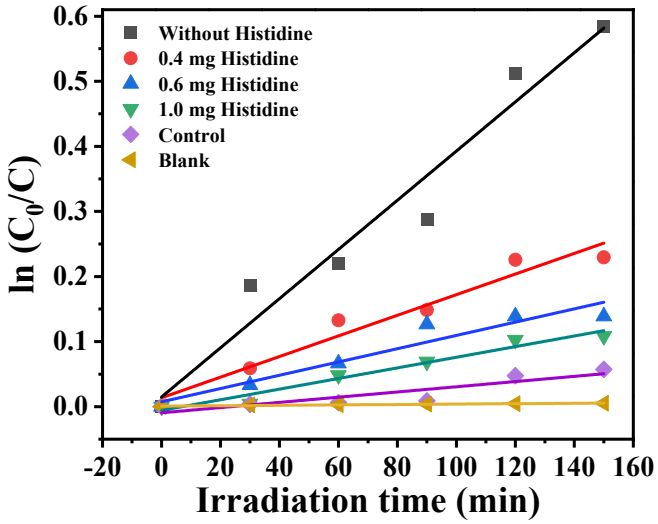

Fig. 8. Degradation kinetics of **β-naphthol** treated with 0.2 mg/mL of Mg OH)$_2$/CdSheteronanostructures in presence of ROS scavenger histidine, confirmed the role of ROS toward **β-naphthol** degradation

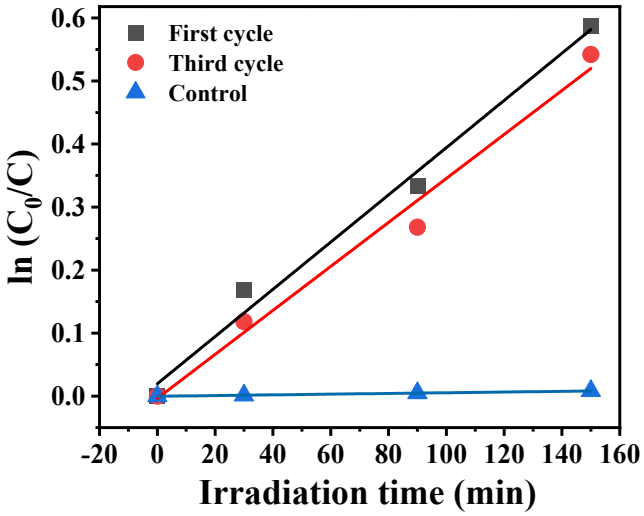

Fig. 9. Re-usability of Mg (OH)$_2$/CdSheteronanostructures in **β-naphthol** degradation

experiment was designed to scavenge the generated ROS in the β-naphthol solution by histidine, which is a well-known scavenger of hydroxyl radicals and singlet oxygen [39]. However, in this study, it is important to ascertain that histidine itself does not exhibit any photocatalytic activity. In this regard, a control experiment is kept which resulted in negligible degradation of pollutant treated with 1.0 mg of histidine per 30 mL of the solution without photocatalyst (Mg (OH)$_2$/CdS heteronanostructures), illuminated by natural sunlight. The extent of degradation was similar to the blank sample comprising pollutant illuminated under natural sunlight, without histidine and photocatalyst (Fig. 8). Degradation efficiencies of the test sample comprising 0.2 mg/mL of photocatalyst (Mg (OH)$_2$/CdS heteronanostructures) in β-naphthol solution, illuminated with natural sunlight, decreased with an increase in the histidine concentration (0.4 mg/30 mL to 1.0 mg/30 mL in β-naphthol solution). Notably, the batch of β-naphthol solution treated with 1.0 mg/30 mL histidine showed 80% inhibition of photodegradation as compared to the batch without histidine addition. These results, together with the terephthalic acid assay confirmed

ROS-induced mechanism for photodegradation of β-naphthol**.** The time-dependent kinetic study of the test solution was carried out using the same UV-visible spectrophotometer. All of the analyses were performed in triplicate and the obtained results are represented as a mean and standard deviation of three analyses.

Reusability and Stability of the Mg $(OH)_2$/ CdSheteronanostructures

After the β-naphthol degradation, the catalyst was separated from the reaction flask through centrifugation, washed several times with water, and reused for the next cycle. The reusability of the catalyst towards the β-naphthol degradation was monitored by UV/Vis spectroscopy, and the results of up to three cycles are shown in Fig. 9. For the catalytic degradation of β-naphthol, the catalytic activities decreased by 3 and 4 %, respectively, after three cycles; therefore, the Mg $(OH)_2$/CdSheteronanostructures have high stability, reusability, and applicability for practical applications.

CONCLUSIONS

A novel and facile nanoscale photocatalyst Mg $(OH)_2$/CdS was developed by precipitation method, which exhibited enhanced photodegradation of a model pollutant– β-naphthol. The FE-SEM images of Mg $(OH)_2$/ CdS samples exhibited a cauliflower-shaped structure in some portions, whereas Mg $(OH)_2$ showed bristle-shaped nanoneedles. The length of Mg $(OH)_2$nanoneedles is about 1000 nm and the diameter is 20 ± 5 nm. The photocatalyst concentration of 0.2 mg/mL, at pH 8.5 was optimum for photocatalytic degradation of β-naphthol. The degradation efficiency of β-naphthol depended on photocatalyst concentration, sunlight illumination. The photodegradation phenomenon was attributed to the generation of hydroxyl radicals, favored by a blue shift in the bandgap absorption of CdS. The role of ROS generation towards photocatalytic activity was proved by showing an increase in the generation of OH^* by terephthalic acid assay. The higher catalytic activity of MC2 is attributed to the synergistic interaction between Mg $(OH)_2$ and CdS and efficient charge separation. The present synthetic method is inexpensive and the synthesized Mg $(OH)_2$/CdS hetero nanostructures could not only be used as a well visible photocatalyst but also as an efficient photothermal material.

DECLARATION OF COMPETING INTEREST

The authors declare that they have no known competing financial interests or personal relationships that could have appeared to influence the work reported in this paper

ACKNOWLEDGMENTS

The authors are thankful to Indira Gandhi Delhi Technical University for Women for providing the facilities. The authors also give thanks to the Centre for Nanoscience and Nanotechnology, Jamia Millia Islamia, New Delhi, and for providing the instrumental facilities.

APPENDIX A. SUPPLEMENTARY DATA

Supplementary data to this article can be found online at http://www.jwent.net/.

REFERENCES

1. Ahmad A, Mohd-Setapar SH, Chuong CS, Khatoon A, Wani WA, Kumar R, et al. Recent advances in new generation dye removal technologies: novel search for approaches to reprocess wastewater. RSC Advances. 2015;5(39):30801-18.
2. Zhang Y, Wu B, Xu H, Liu H, Wang M, He Y, et al. Nanomaterials-enabled water and wastewater treatment. NanoImpact. 2016;3-4:22-39.
3. Luévano-Hipólito E, Torres Martínez LM. Mg(OH)2 Films Prepared by Ink-Jet Printing and Their Photocatalytic Activity in CO2 Reduction and H2O Conversion. Topics in Catalysis. 2018;61(15-17):1574-84.
4. Ecker M (2004) Purification of liquids, especially water containing heavy metal ions, involves bonding the impurities on or in magnesium hydroxide. DE 10318746-A1.
5. Sirota V, Selemenev V, Kovaleva M, Pavlenko I, Mamunin K, Dokalov V, et al. Preparation of crystalline Mg(OH)2 nanopowder from serpentinite mineral. International Journal of Mining Science and Technology. 2018;28(3):499-503.
6. Raza SM, Rizwan Ali S, Naeem M, Uddin Z, Qaseem S, Imran Ali S, et al. Tuning the bandgap in Co-doped Mg(OH)2 nanoparticles. International Journal of Modern Physics B. 2019;33(17):1950182.
7. Kumari L, Li WZ, Vannoy CH, Leblanc RM, Wang DZ. Synthesis, characterization and optical properties of Mg(OH)2 micro-/nanostructure and its conversion to MgO. Ceramics International. 2009;35(8):3355-64.
8. Yagmurcukardes M, Torun E, Senger RT, Peeters FM, Sahin H. Mg(OH)2–WS2 van der Waals heterobilayer: Electric field tunable band-gap crossover. Physical Review B. 2016;94(19).
9. Bacaksiz C, Dominguez A, Rubio A, Senger RT, Sahin H. h-AlN-Mg(OH)2 van der Waals bilayer heterostructure: Tuning the excitonic characteristics. Physical Review B. 2017;95(7).
10. Wang B-J, Li X-H, Cai X-L, Yu W-Y, Zhang L-W, Zhao R-Q, et al. Blue Phosphorus/Mg(OH)2 van der Waals Heterostructures as Promising Visible-Light Photocatalysts for Water Splitting. The Journal of Physical Chemistry C.

2018;122(13):7075-80.
11. Zheng X, Mao Y, Wen J, Fu X, Liu X. CuInS(2)/Mg(OH)(2) Nanosheets for the Enhanced Visible-Light Photocatalytic Degradation of Tetracycline. Nanomaterials (Basel). 2019;9(11):1567.
12. Liu M, Wang Y, Chen L, Zhang Y, Lin Z. Mg(OH)2 Supported Nanoscale Zero Valent Iron Enhancing the Removal of Pb(II) from Aqueous Solution. ACS Applied Materials & Interfaces. 2015;7(15):7961-9.
13. Li Y, Tian C, Liu W, Xu S, Xu Y, Cui R, et al. Carbon Cloth Supported Nano-Mg(OH)(2) for the Enrichment and Recovery of Rare Earth Element Eu(III) From Aqueous Solution. Front Chem. 2018;6:118-.
14. Zeng X-F, Han X-W, Chen B, Wang M, Zhang L-L, Wang J-X, et al. Facile synthesis of Mg(OH)2/graphene oxide composite by high-gravity technology for removal of dyes. Journal of Materials Science. 2017;53(4):2511-9.
15. Šťastný M, Štengl V, Henych J, Tolasz J, Kormunda M, Ederer J, et al. Synthesis and characterization of TiO2/Mg(OH)2 composites for catalytic degradation of CWA surrogates. RSC Advances. 2020;10(33):19542-52.
16. KongN, Han B, Li Z, Fang Y, Feng K, Wu Z. et al (2020) Ru Nanoparticles Supported on Mg(OH)2 Microflowers as Catalysts for Photothermal Carbon Dioxide Hydrogenation. ACS Applied Nano Materials3(3):3028–3033. https://pubs.acs.org/doi/10.1021/acsanm.0c00383
17. Ichimura M. Impurity Doping in Mg(OH)(2) for n-Type and p-Type Conductivity Control. Materials (Basel). 2020;13(13):2972.
18. Venkatesh N, Sabarish K, Murugadoss G. Thangamuthu R, Sakthivel P (2020) Visible light–driven photocatalytic dye degradation under natural sunlight using Sn-doped CdS nanoparticles. Environ Sci Pollut Res 27:43212–43222 (2020). https://doi.org/10.1007/s11356-020-10268-3
19. Das PS, Das S, Ghosh J, Mukhopadhyay AK. Unique Microstructure of 3D Self-Assembled Mg(OH)2 Nanoparticles for Methylene Blue Degradation in Presence of Direct Sun Light. Transactions of the Indian Ceramic Society. 2018;77(4):226-34.
20. Sethi YA, Panmand RP, Ambalkar AA, Kulkarni AK (2019) In situ preparation of CdS decorated ZnWO4 nanorods as a photocatalyst for direct conversion of sunlight into fuel and RhB degradation. Sustain Energy Fuels 3:793-800. https://doi.org/10.1039/C8SE00632F
21. Ijadpanah-Saravi H, Dehestaniathar S, Khodadadi A, Safari M. Optimization of photocatalytic degradation of β-naphthol using nano TiO2-activated carbon composite. Desalination and Water Treatment. 2014:1-12.
22. Qu X, Alvarez PJJ, Li Q. Applications of nanotechnology in water and wastewater treatment. Water Research. 2013;47(12):3931-46.
23. Hamal DB, Klabunde KJ. Valence State and Catalytic Role of Cobalt Ions in Cobalt TiO2 Nanoparticle Photocatalysts for Acetaldehyde Degradation under Visible Light. The Journal of Physical Chemistry C. 2011;115(35):17359-67.
24. Chen Y, Zhou T, Fang H, Li S, Yao Y, He Y. A Novel Preparation of Nano-sized Hexagonal Mg(OH)2. Procedia Engineering. 2015;102:388-94.
25. Liu P, Guo J. Organo-modified magnesium hydroxide nano-needle and its polystyrene nanocomposite. Journal of Nanoparticle Research. 2006;9(4):669-73.
26. Chen Y-Y, Yu S-H, Yao Q-Z, Fu S-Q, Zhou G-T. One-step synthesis of Ag2O@Mg(OH)2 nanocomposite as an efficient scavenger for iodine and uranium. Journal of Colloid and Interface Science. 2018;510:280-91.
27. Moholkar AV, Agawane GL, Sim K-U, Kwon Y-b, Choi DS, Rajpure KY, et al. Temperature dependent structural, luminescent and XPS studies of CdO:Ga thin films deposited by spray pyrolysis. Journal of Alloys and Compounds. 2010;506(2):794-9.
28. Rajeshwar K, de Tacconi NR, Chenthamarakshan CR. Semiconductor-Based Composite Materials: Preparation, Properties, and Performance. Chemistry of Materials. 2001;13(9):2765-82.
29. Chang S-Y, Liu L, Asher SA. Preparation and Properties of Tailored Morphology, Monodisperse Colloidal Silica-Cadmium Sulfide Nanocomposites. Journal of the American Chemical Society. 1994;116(15):6739-44.
30. Zhang C-F, Qiu L-G, Ke F, Zhu Y-J, Yuan Y-P, Xu G-S, et al. A novel magnetic recyclable photocatalyst based on a core–shell metal–organic framework Fe3O4@MIL-100(Fe) for the decolorization of methylene blue dye. Journal of Materials Chemistry A. 2013;1(45):14329.
31. Zhao W, Bai Z, Ren A, Guo B, Wu C. Sunlight photocatalytic activity of CdS modified TiO2 loaded on activated carbon fibers. Applied Surface Science. 2010;256(11):3493-8.
32. El-Kemary M, Abdel-Moneam Y, Madkour M, El-Mehasseb I. Enhanced photocatalytic degradation of Safranin-O by heterogeneous nanoparticles for environmental applications. Journal of Luminescence. 2011;131(4):570-6.
33. Herrmann J-M. Heterogeneous photocatalysis: fundamentals and applications to the removal of various types of aqueous pollutants. Catalysis Today. 1999;53(1):115-29.
34. Applerot G, Lipovsky A, Dror R, Perkas N, Nitzan Y, Lubart R, et al. Enhanced Antibacterial Activity of Nanocrystalline ZnO Due to Increased ROS-Mediated Cell Injury. Advanced Functional Materials. 2009;19(6):842-52.
35. Nenavathu BP, Krishna Rao AVR, Goyal A, Kapoor A, Dutta RK. Synthesis, characterization and enhanced photocatalytic degradation efficiency of Se doped ZnO nanoparticles using trypan blue as a model dye. Applied Catalysis A: General. 2013;459:106-13.